small NANO MICRO

Fluorescence Imaging

Lipid-PEG-Folate Encapsulated Nanoparticles with Aggregation Induced Emission Characteristics: Cellular Uptake Mechanism and Two-Photon Fluorescence Imaging

*Junlong Geng, Kai Li, Dan Ding, Xinhai Zhang, Wei Qin, Jianzhao Liu, Ben Zhong Tang, and Bin Liu**

***F**olate functionalized nanoparticles (NPs) that contain fluorogens with aggregation-induced emission (AIE) characteristics are fabricated to show bright far-red/near-infrared fluorescence, a large two-photon absorption cross section and low cytotoxicity, which are internalized into MCF-7 cancer cells mainly through caveolae-mediated endocytosis. One-photon excited in vivo fluorescence imaging illustrates that these AIE NPs can accumulate in a tumor and two-photon excited ex vivo tumor tissue imaging reveals that they can be easily detected in the tumor mass at a depth of 400 μm. These studies indicate that AIE NPs are promising alternatives to conventional TPA probes for biological imaging.*

1. Introduction

Fluorescence imaging techniques have been intensely used in biological studies as well as disease diagnosis and treatment because of their high sensitivity and relatively inexpensive and more maneuverable equipments.[1] As compared to traditional one-photon fluorescence imaging, two-photon fluorescence imaging techniques have shown advantages such as minimal phototoxicity to living biosubstrate, deeper tissue/tumor penetration depth and lower interference from biosubstrate autofluorescence.[2] To achieve high resolution and good contrast in practice, two-photon absorbing probes with large two photon absorption (TPA) cross section (δ) and high quantum yield (η) to afford efficient two photon action cross section ($\eta\delta$) remain in urgent demand. Among various classes of TPA materials, organic TPA chromophores have attracted great interest due to their feasible preparation, abundant versatility and good biocompatibility.[3] However, the prerequisite condition for these organic soluble TPA materials to be used for biological applications is the water-solubility. As compared to the sophisticated approach to synthesize each water-soluble TPA molecule,[4] fabrication of nanoparticles (NPs) offers a more general strategy to yield water dispersable TPA materials with surface functionalization for targeted bioimaging. To date, a number of organic-soluble TPA chromophores have been synthesized to possess large $\eta\delta$ values in organic solvents, but suffer from sudden decrease in $\eta\delta$ upon NP formulation in aqueous media, which is mainly caused by aggregation induced fluorescence quenching due to π–π stacking and other nonradiative pathways.[5]

To solve this problem, we and others have developed a variety of organic chromophores with aggregation-induced

Prof. B. Liu, J. Geng, Dr. D. Ding
Department of Chemical and Biomolecular Engineering
National University of Singapore
Singapore 117576
Fax: (+65) 6779-1936
E-mail: cheliub@nus.edu.sg; liub@imre.a-star.edu.sg
Prof. B. Liu, Prof. B. Z. Tang, Dr. K. Li, Dr. X. Zhang
Institute of Materials Research Engineering
3 Research Link, 117602, Singapore
W. Qin, Dr J. Liu, Prof. B. Z. Tang
Department of Chemistry
Institute for Advanced Study
Division of Biomedical Engineering
State Key Laboratory of Molecular Neuroscience
and Institute of Molecular Functional Materials
The Hong Kong University of Science and Technology
Clear Water Bay, Kowloon, Hong Kong, China

DOI: 10.1002/smll.201200814

© 2012 Wiley-VCH Verlag GmbH & Co. KGaA, Weinheim

emission (AIE) signature.[6] These AIE luminogens show great potential in construction of NPs with high quantum yield due to restriction of intermolecular vibrational and rotational motions in the nanoaggregates.[6] In the past, different strategies have been developed for fabrication of AIE NPs with high TPA cross sections for bioimaging applications.[7,8] Unfortunately, majority of AIE NPs has emission wavelength below 650 nm, which greatly limits their application in tissue and tumor imaging due to the potential interference of probe optical absorption and auto fluorescence from the biosubstrate.[9] In addition, although AIE nanoaggregates with far-red/near-infrared (FR/NIR) emission (>650 nm) have been successfully demonstrated,[10] the reported bare nanoaggregates have relatively large size (~150 nm) and are not suitable for targeted cellular imaging due to the lack of surface functional groups.

In this contribution, we report the synthesis of AIE NPs with high TPA cross-section and FR/NIR emission for one-photon excited *in vitro* and *in vivo* and two-photon excited *ex vivo* fluorescence imaging. 2-(2,6-Bis((*E*)-4-(phenyl(4′-(1,2,2-triphenylvinyl)-[1,1′-biphenyl]-4-yl)amino)styryl)-4*H*-pyran-4-ylidene) malononitrile (TPE-TPA-DCM) was selected as the luminogen because it shows AIE features with high brightness in FR/NIR region.[11] The NPs were prepared with nanoprecipitation method using a mixture of lipid derivatives, 1,2-distearoyl-*sn*-glycero-3-phosphoethanolamine-*N*-[methoxy(polyethylene glycol)-2000] (DSPE-PEG_{2000}) and DSPE-PEG_{5000}-folate, as the encapsulation matrix. Such a lipid-PEG formulation has been actively used in encapsulation of versatile chromophores to afford stable fluorescent probes due to their good biocompatibility.[8,12] To understand the effect of formulation on cellular uptake of fluorescent probes, cellular uptake mechanism of the as-prepared lipid-PEG encapsulated NPs has been investigated for the first time. In addition, the targeting ability of the obtained NPs to both folate receptor-overexpressed cancer cells and tumors has been examined. Furthermore, *ex vivo* two-photon excited tumor imaging was further performed to investigate the effective penetration depth of the AIE NPs upon two-photon excitation at 800 nm. These results indicate that the lipid-PEG encapsulated AIE NPs can serve as efficient fluorescent probes for both one-photon and two-photon excited fluorescence imaging.

2. Results and Discussion

2.1. Synthesis and Characterization of TPE-TPA-DCM Loaded DSPE-PEG NPs

The chemical structure of TPE-TPA-DCM is shown as the inset in **Figure 1**.[11] The fluorescent properties of TPE-TPA-DCM in nanoaggregates were investigated by monitoring the emission of TPE-TPA-DCM in tetrahydrofuran (THF) upon addition of different amount of water. As shown in Figure 1, upon gradual addition of water into THF solution, the fluorescence intensity of TPE-TPA-DCM is significantly weakened at the initial stage, which is mainly caused by the

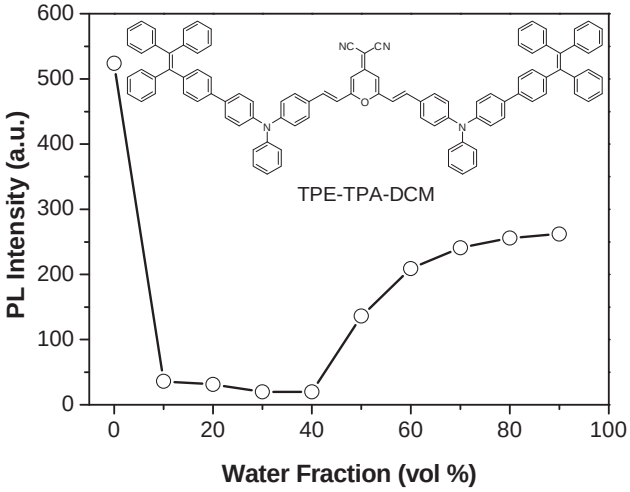

Figure 1. Changes of the maximum photoluminescence (PL) intensity of TPE-TPA-DCM *vs.* water fraction in THF/water mixtures ([TPE-TPA-DCM] = 10 μM; λ_{ex} = 480 nm). The inset shows the chemical structure of TPE-TPA-DCM.

increase in solvent polarity and the charge transfer between the excited state of TPE-TPA-DCM and polar solvents.[11] The turning point appears at the water volume fraction (f_w) of 50%, after which the fluorescence intensity increases with further addition of water up to 90%, indicating the AIE characteristic of TPE-TPA-DCM.

The folic acid-functionalized TPE-TPA-DCM loaded NPs (FTTDNPs) were synthesized using a modified nanoprecipitation method.[12] The chemical structures of materials used for FTTDNP formation are illustrated in **Scheme 1**. One starts with a THF solution containing TPE-TPA-DCM, DSPE-PEG_{2000} and DSPE-PEG_{5000}-folate (50 mol% of the matrix). Upon mixing the THF solution with water under sonication, the hydrophobic DSPE segments tend to entangle with hydrophobic TPE-TPA-DCM molecules and the hydrophilic PEG chains extend into the aqueous phase. After evaporation of THF overnight, the FTTDNP suspension was collected after further purification using a 0.2 μm syringe filter. No obvious precipitation from the FTTDNP suspension was observed after storage at 4 ºC for 5 months, indicating excellent colloidal stability of the as-prepared NPs. As a control group, DSPE-PEG_{2000} encapsulated TPE-TPA-DCM NPs (TTDNPs) or 4-(dicyanomethylene)-2-methyl-6-(p-dimethylaminostyryl)-4H-pyran (DCM) NPs without surface folic acid were also synthesized following the same procedure.

Laser light scattering results suggest that FTTDNPs and TTDNPs have similar volume average hydrodynamic diameters, which are 53 ± 2 nm and 51 ± 2 nm, respectively. The morphology of FTTDNPs was investigated using field emission transmission electron microscopy (FE-TEM), which is shown in **Figure 2**a. The image reveals that the FTTDNPs are spherical and can be clearly distinguished as dark dots due to the high electron density of TPE-TPA-DCM molecule. Figure 2b shows the UV-vis absorption and photoluminescence (PL) spectra of FTTDNPs in water suspension. FTTDNPs show two maximum absorption peaks at 354 nm and 497 nm, respectively. The emission maximum appears

© 2012 Wiley-VCH Verlag GmbH & Co. KGaA, Weinheim

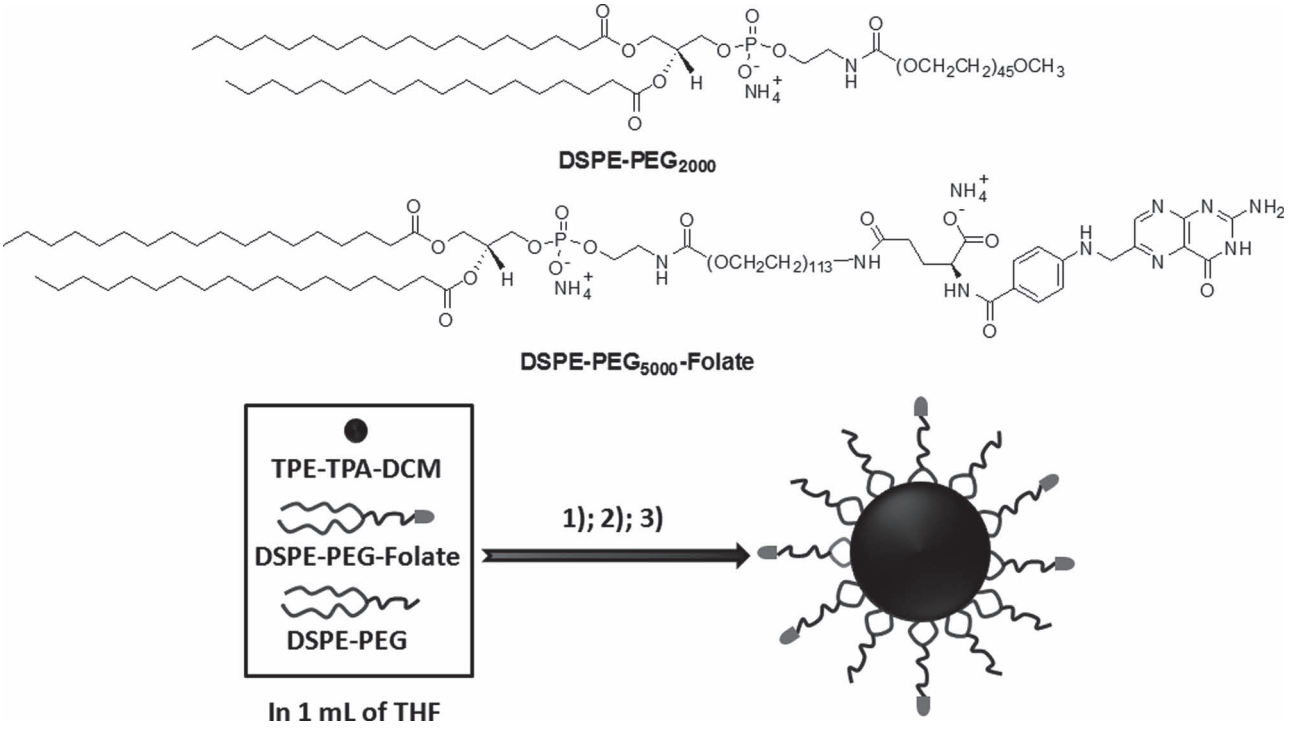

Scheme 1. Chemical structures of DSPE-PEG_{2000} and DSPE-PEG_{5000}-folate, and schematic illustration of the synthesis of FTTDNPs. Conditions: 1) Mix with 9 mL of H_2O; 2) Sonication for 60 s; 3) Solvent evaporation.

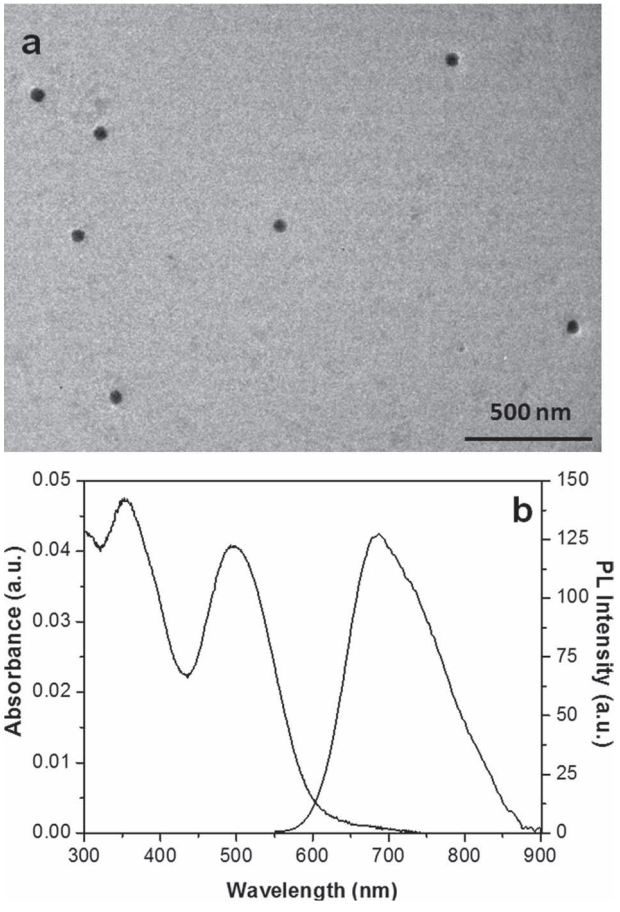

Figure 2. (a) FE-TEM image of the FTTDNPs. (b) UV-vis absorption and PL spectra of FTTDNPs in water (λ_{ex} = 497 nm).

at 684 nm with an intense emission tail extended to over 850 nm. The FR/NIR emission and large Stokes shift make them good candidates for both *in vitro* and *in vivo* fluorescence imaging. The η of FTTDNPs in water is 0.13, which is over 10 times higher as compared to that of DCM NPs (~0.01), measured using DCM in methanol as a standard (η = 0.43).[13] This further demonstrates the importance of molecular design that the conjugation of triphenylamine and tetraphenylethylene to the DCM core has significantly transfromed a traditional chromophore with aggregation induced quenching to a AIE luminogen.[11] It is also important to note that such modification does not significanlty alter the absorption and emission maxima of DCM (Figure S1 in the Supporting Information, SI).

2.2. Two-photon Absorbing Property of FTTDNPs

The TPA spectra of FTTDNP water suspension were studied using the two-photon-induced fluorescence (TPIF) technique with a femtosecond pulsed laser source. According to the laser availability, the spectra were collected in 800 nm to 960 nm range at 10 nm intervals. The relative TPIF intensities of FTTDNPs were measured using Rhodamine 6G in methanol as the standard. Details of the measurement and calculation method are provided in the Experimental Section.[14] The TPA cross section was calculated based on NP concentration and the obtained TPA spectrum of FTTDNPs is shown in **Figure 3**. The relationship between [FTTDNP] and [TPE-TPA-DCM] is shown in the SI. The maximum δ is ~2.3 × 10^6 GM at 820 nm, which gives an $\eta\delta$ value of 2.8 × 10^5 GM. The result suggests that FTTDNPs have larger TPA

 © 2012 Wiley-VCH Verlag GmbH & Co. KGaA, Weinheim

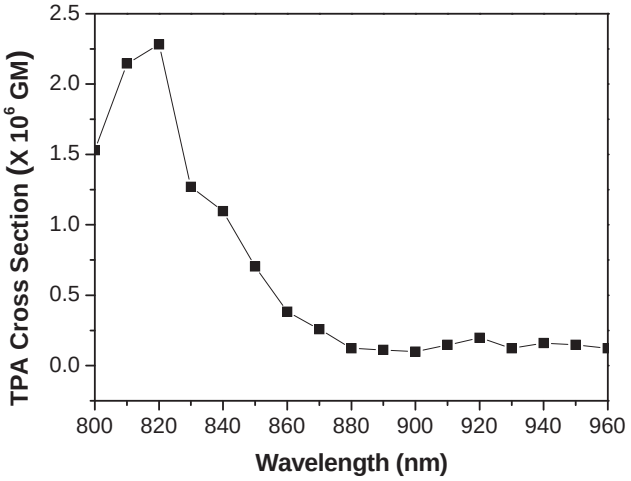

Figure 3. Two-photon absorption spectrum of FTTDNPs in water.

cross-sections than previously reported NPs (e.g., organic dye nanoaggregates and quantum dots) in aqueous media,[15] which is highly desirable to ensure a high signal-to-noise ratio in bioimaging experiment.

2.3. Uptake Mechanism of FTTDNPs

The application of FTTDNPs for *in vitro* cellular imaging was studied by confocal laser scanning microscopy with MCF-7 breast cancer cells as an example. The confocal images of MCF-7 breast cells after incubation with both FTTDNP and TTDNP suspension are shown in **Figures 4**a and 4b, respectively. The cell nuclei were stained with 4,6-diamidino-2-phenylindole (DAPI). These images were taken upon excitation at 488 nm with a 650 nm long pass barrier filter. The higher fluorescence intensity observed in Figure 4a as compared to that in Figure 4b indicates that more FTTDNPs are internalized into MCF-7 breast cells *via* folate receptor-mediated endocytosis.[16] 3D sectional confocal image of the control group indicates that the fluorescene is mainly from the cytoplasm due to the sufficient uptake (Figure S2 in the SI).

The folate receptor-mediated endocytosis mechanism has been further examined by free folic acid blocking and temperature dependent MCF-7 cellular uptake studies, using the cells incubated with FTTDNPs at 37 °C as a control (Figure 4a).[17] The folic acid blocking experiment was conducted by treating the MCF-7 breast cancer cells with free folic acid, followed

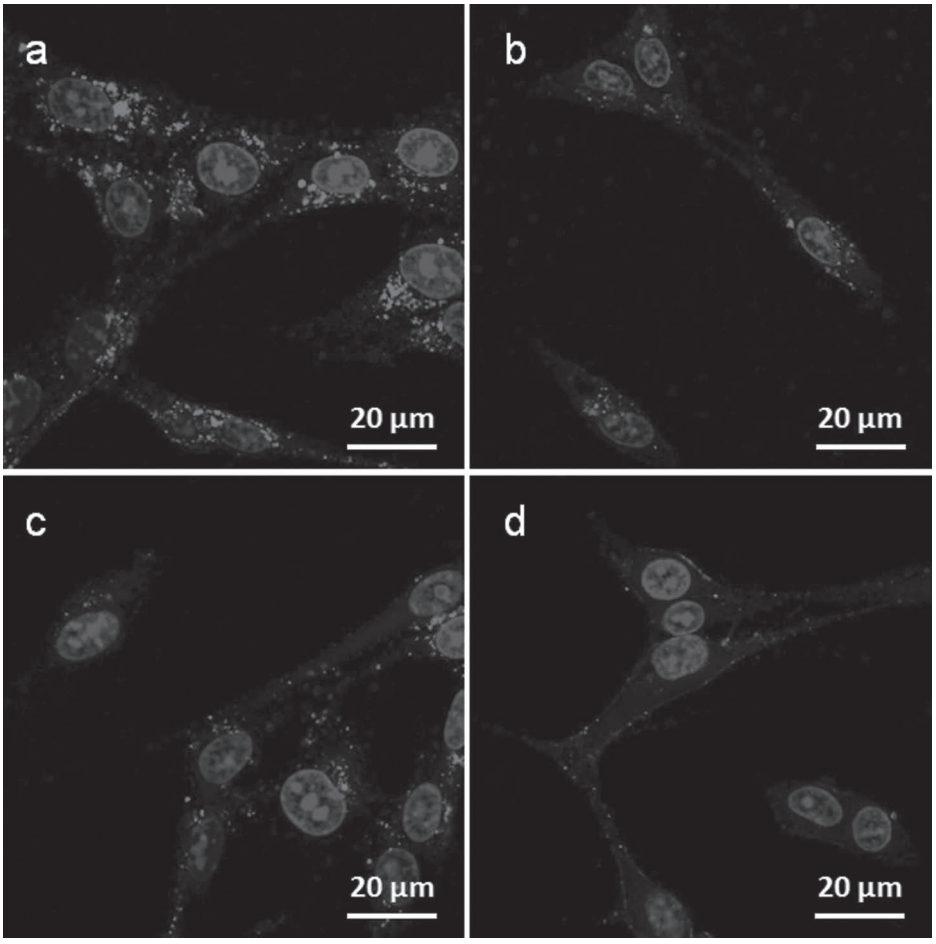

Figure 4. Confocal fluorescence images of MCF-7 breast cancer cells after 2 h incubation with (a) FTTDNP and (b) TTDNP suspensions at 0.1 nM NPs at 37 °C. (c) Confocal fluorescence image of the free folic acid pre-treated MCF-7 breast cancer cells after 2 h incubation with 0.1 nM FTTDNPs at 37 °C. (d) Confocal fluorescence image of MCF-7 breast cancer cells after 2 h incubation with 0.1 nM of FTTDNPs at 4 °C. The nuclei were stained with 4,6-diamidino-2-phenylindole (DAPI). The images were taken upon excitation at 488 nm with a 650 nm long pass barrier filter. The colour version of Figure 4 can be found in the Supporting Information.

© 2012 Wiley-VCH Verlag GmbH & Co. KGaA, Weinheim

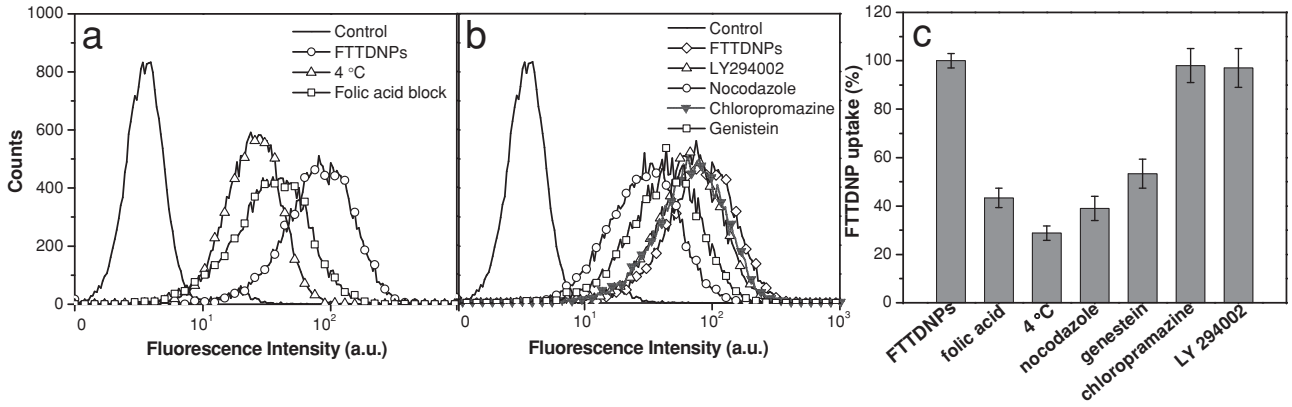

Figure 5. (a) Flow cytometry histograms of pure MCF-7 breast cancer cells without FTTDNP incubation (black) as well as untreated cells at 37 °C (circle), 4 °C (triangle) and free folic acid pre-treated cells (cube) at 37 °C after incubation with 0.1 nM FTTDNPs for 2 h. (b) Flow cytometry histograms of pure MCF-7 breast cancer cells without FTTDNP incubation (black) as well as untreated cells (rhombus), cells treated using endocytic inhibitors of LY284002 (triangle), nocodazole (circle), chloropromazine (del triangle) and genistein (cube) after incubation with 0.1 nM FTTDNPs at 37 °C for 2 h, respectively. (c) Summary of the relative cellular uptake efficiencies under different conditions.

by incubation with 0.1 nM FTTDNP suspension. The corresponding image is shown in Figure 4c, which has a much lower fluorescence intensity as compared to that in Figure 4a, indicating that the uptake of FTTDNPs is greatly inhibited by free folic acid treatment. This should be attributed to the effective blocking of the folate receptors on cell membrane by the free folic acid, which lead to reduced interaction with FTTDNPs and lower uptake efficiency.[17a,c] In addition, the much lower fluorescent signal from Figure 4d as compared to that in Figure 4a suggests that the internalization of FTTDNPs at 4 °C is dramatically inhibited, indicating that the uptake of FTTDNPs by MCF-7 cells is through an energy dependent pathway.[17b] The fluorescent profiles of these samples have also been quantitatively studied using flow cytometry and the results are shown in **Figure 5**a. The relative cellular uptake efficiencies of FTTDNPs under different conditions as compared to the control are shown in Figure 5c. The results show significant inhibition of FTTDNPs uptake by free folic acid block (reduced by 57%) and low temperature (reduced by 71%), which further confirm the receptor-mediated endocytosis pathway.

To date, various endocytic mechanisms are found to be operative in cellular uptake, which include clathrin-mediated endocytosis, caveolae-mediated endocytosis, clathrin- and caveolae-independent endocytosis, and macropinocytosis.[18] To determine the specific uptake mechanism of FTTDNPs, we examined the effect of a series of inhibitors which are known to block corresponding cellular uptake pathways. In these experiments, MCF-7 breast cancer cells were pre-treated with various inhibitors before incubation with 0.1 nM FTTDNP suspension. The cellular uptake efficiencies upon different pre-treatments were quantitatively evaluated with flow cytometry and the results are summarized in Figures 5b and 5c, using untreated cells as the control. A decrease in the average fluorescence intensity due to specific inhibitor treatment reflects involvement of the corresponding endocytic mechanism.[19] As shown in Figure 5c, a moderate decrease of FTTDNP uptake effeciency is observed for nocodazole and genistein pre-treated cells. In addition, no obvious change in FTTDNP uptake is observed upon pre-treatment using chlorpromazine, a clathrin-mediated endocytosis inhibitor.[19] As nocodazole is able to inhibit caveolae-mediated endocytosis and genistein can inhibit both clathrin- and caveolae-mediated endocytosis,[19a,b] these results indicate that FTTDNP uptake by MCF-7 breast cancer cells mainly involves caveolae- rather than clathrin-mediated endocytosis. Moreover, no obvious inhibition by LY294002 suggests that macropinocytosis is not involved.[19c] As folic acid uptake has been considered through binding with folate receptors that are clustered in invaginated caveolae,[20] the folic acid groups functionalized on FTTDNP surface provide the main route to enter MCF-7 cells through caveolae-mediated endocytosis.

In addition, methylthiazolyldiphenyltetrazolium (MTT) assay was adapted to investigate the cytotoxicity of FTTDNPs by studying the metabolic viability of MCF-7 breast cancer cells after incubation with FTTDNPs at various TPE-TPA-DCM concentrations. As shown in **Figure 6**, the cell viability remains 95% within 48 h under the experimental conditions, indicating the low cytotoxicity of FTTDNPs, which will benefit both *in vitro* and *in vivo* fluorescence imaging.

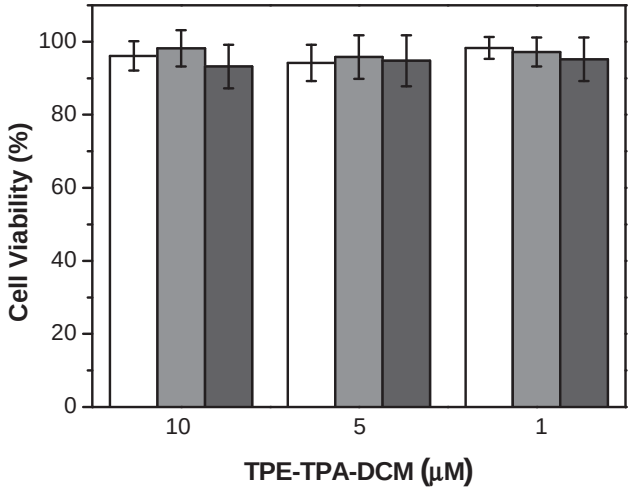

Figure 6. Metabolic viability of MCF-7 breast cancer cells after incubation with FTTDNPs at various TPE-TPA-DCM concentrations for 12 (blank), 24 (gray) and 48 h (dark gray).

© 2012 Wiley-VCH Verlag GmbH & Co. KGaA, Weinheim

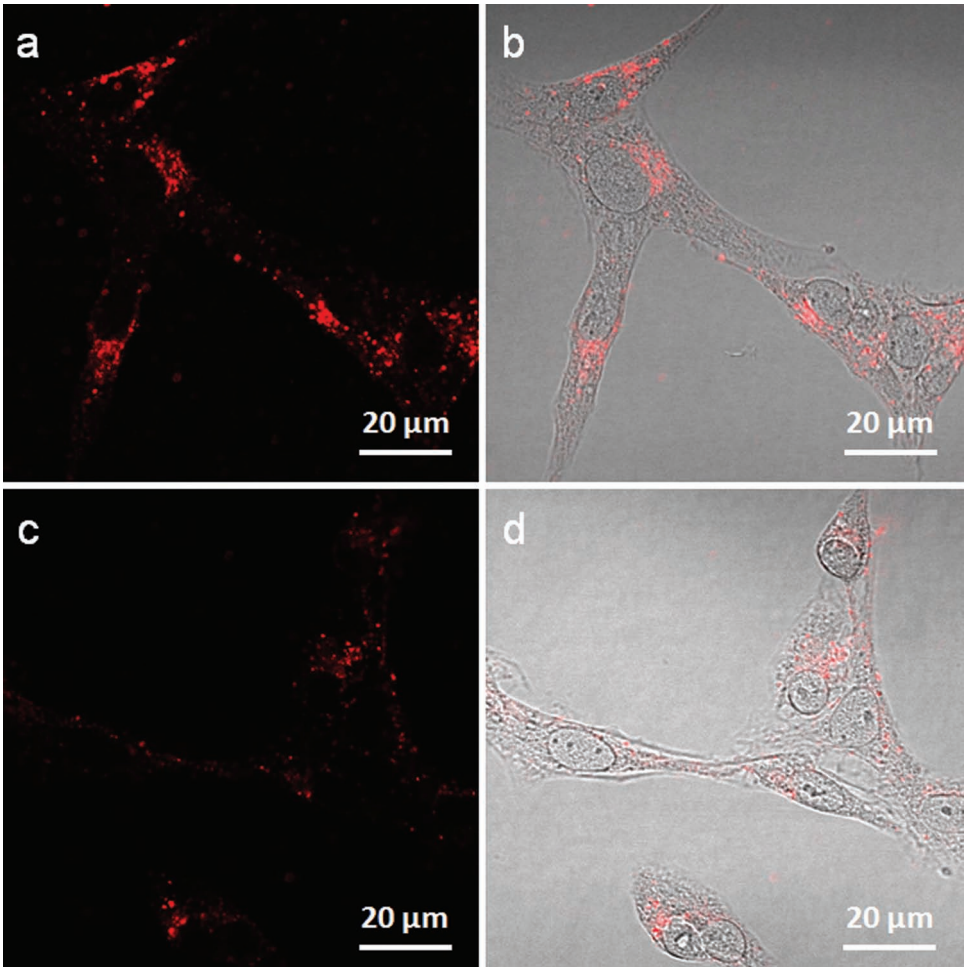

Figure 7. Two-photon excited fluorescence imaging of MCF-7 breast cancer cells after 2 h incubation with (a,b) FTTDNP and (c,d) TTDNP suspensions in culture medium with 0.1 nM NPs at 37 °C, respectively. The images were recorded upon 800 nm excitation with 600–780 nm band pass filter. The colour version of Figure 7 can be found in the Supporting Information.

2.4. Two-Photon Excited Cell Imaging

Two-photon fluorescence images of MCF-7 breast cancer cells after incubation with FTTDNP and TTDNP suspensions in culture medium with 0.1 nM NPs are shown in **Figure 7**. The fluorescent signal from cytoplasm is clearly observed to distinguish the cell profile, indicating that FTTDNPs can serve as a promising two-photon fluorescent probe. Under the same experimental conditions, the cells show no auto fluorescence (Figure S3 in the SI). The higher fluorescence intensity observed in Figure 7a as compared to that in Figure 7c further confirms that more FTTDNPs are internalized into MCF-7 breast cancer cells *via* folate receptor-mediated endocytosis,[16] which is consistent with the results shown in Figures 5a and 5b.

2.5. One-photon Excited *In Vivo* and Two-photon Excited *Ex Vivo* Fluorescence Imaging

The *in vitro* studies demonstrated the targeting ability of FTTDNPs to MCF-7 breast cancer cells, which motivated us to further investigate their *in vivo* performance. Mice bearing murine hepatoma H22 tumors with overexpressed folate receptors were administrated with FTTDNP and TTDNP suspension *via* tail vein injection. The mice were imaged at different time points post injection, using a Maestro EX *in vivo* fluorescence imaging system. **Figure 8**A and 8B show the time-dependent excretion profile and tumor accumulation of both FTTDNPs and TTDNPs in tumor-bearing mice, respectively. After 1h, the fluorescence signal from FTTDNPs was detected in the tumor site. A steady increase of the tumor fluorescence intensity in the mice injected with FTTDNPs was observed in the following 6h and 12h. Moreover, the tumor site of the mouse treated with FTTDNPs (Figure 8A) shows much higher fluorescence intensity as compared to that treated with TTDNPs (Figure 8B) at 12 h post injection. These results indicate that FTTDNPs are able to efficiently accumulate in tumor tissues through both passive targeting by enhanced permeability and retention (EPR) effect and folate receptor-mediated active targeting effect.[16]

The utility of FTTDNPs in deep tissue two-photon excited fluorescence imaging was also investigated in a tumor-bearing mouse model. The model animals were established by subcutaneously inoculating the C6 glioma cancer cells into the left flank of the BALB/c nude mice. After intratumoral injection

© 2012 Wiley-VCH Verlag GmbH & Co. KGaA, Weinheim

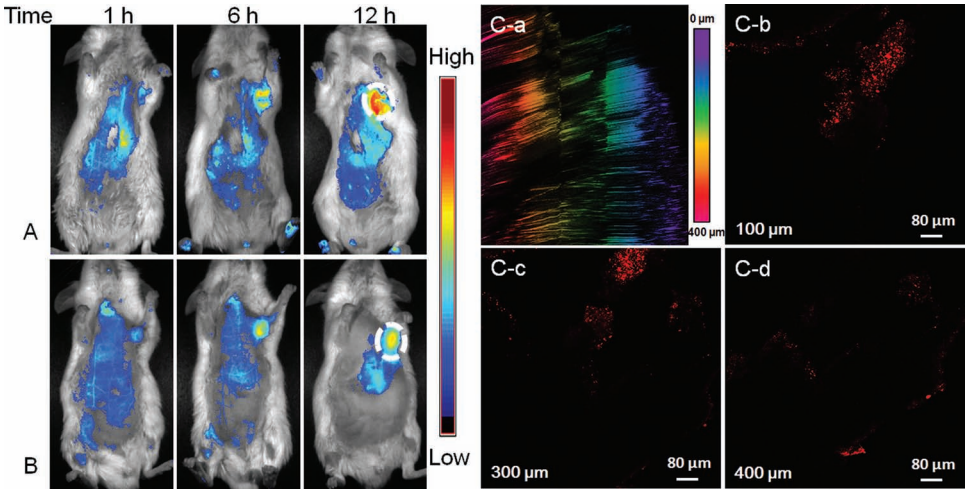

Figure 8. One-photon excited in vivo non-invasive fluorescence imaging of H22 tumor-bearing mice after intravenous injection of A) FTTDNPs and B) TTDNPs at the same NP concentration of 1 nM. The white circles mark the tumor sites. (C-a) 3D two-photon fluorescence image of C6 tumor from the mouse that was intratumorally injected with FTTDNPs. (C-b) 100 μm, (C-c) 300 μm and (C-d) 400 μm deep images from the C6 tumor. The images were recorded upon 800 nm excitation with 600–780 nm band pass filter.

of the FTTDNPs, the C6 tumor-bearing mice were sacrificed at 24 h post-injection. The tumor tissues were isolated, which were then whole-mounted and imaged by two-photon excited fluorescence microscope with 800 nm laser excitation. To investigate the efficient penetration depth of fluorescence from FTTDNPs in tumor mass, the images were taken layer-by-layer in a 3 μm-step. Under the same experimental condition, the tumor shows no auto fluorescence (Figure S4 in the SI). As shown in Figure 8C, the 3D two-photon excited fluorescence image and the images in various depth of tumor mass indicate that deep tumor tissue imaging of at least 400 μm can be achieved. These results demonstrate that the FTTDNPs can also serve as a feasible two-photon absorbing nanoprobes for deep tumor tissue imaging.

3. Conclusion

In summary, we synthesized AIE luminogen-loaded fluorescent NPs for targeted one-photon and two-photon fluorescence imaging of folate receptor overexpressed cancer cells and tumor tissues. The as-prepared NPs show high TPA cross section of 2.3×10^6 GM for each NP, bright FR/NIR fluorescence, small size (~50 nm) and low cytotoxicity. Uptake mechanism study suggests that the fabricated NPs are mainly internalized into MCF-7 breast cancer cells through caveolae-mediated endocytosis. In addition to *in vitro* study, *in vivo* fluorescence imaging illustrates that FTTDNPs can effectively accumulate in tumor tissue for tumor diagnosis in a living body. Moreover, the high TPA cross section and FR/NIR emission of NPs allow two-photon fluorescence imaging of MCF-7 breast cancer cells and ensure the efficient penetration depth in tumor tissue (~400 μm) upon intratumoral injection on a C6 glioma tumor-bearing nude mouse model. The unique two-photon excited FR/NIR fluorescence, efficient live cell internalization and desirable tumor penetration depth make AIE NPs a novel class of fluorescent probes for *in vitro* and *in vivo* imaging and diagnosis in the near future.

4. Experimental Section

Materials: 2-(2,6-Bis((*E*)-4-(phenyl(4′-(1,2,2-triphenylvinyl)-[1,1'-biphenyl]-4-yl)amino) styryl)-4*H*-pyran-4-ylidene) malononitrile (TPE-TPA-DCM) was synthesized according to the literature.[11] 1,2-Distearoyl-*sn*-glycero-3-phosphoethanolamine-*N*-[methoxy(polyethylene glycol)-2000] (DSPE-PEG_{2000}) was a gift from Lipoid GmbH (Ludwigshafen, Germany). DSPE-PEG_{5000}-Folate was a commercial product of Avanti Polar Lipids, Inc. Tetrahydrofuran (THF), 4′,6-diamidino-2-phenylindole (DAPI), 3-(4,5-dimethylthiazol-2-yl)-2,5-diphenyl tetrazolium bromide (MTT), penicillin-streptomycin solution, LY294002, chlorpromazine, genistein, nocodazole, fetal bovine serum (FBS) and trypsin-EDTA solution were purchased from Sigma-Aldrich. Milli-Q water was supplied by Milli-Q Plus System (Millipore Corporation, Breford, USA). MCF-7 breast cancer cells were provided by American Type Culture Collection.

Synthesis of TPE-TPA-DCM Loaded DSPE-PEG NPs: A THF solution (1 mL) containing TPE-TPA-DCM (1 mg) and a mixture of DSPE-PEG_{2000} and DSPE-PEG_{5000}-folate (1.5 mg; molar ratio of DSPE-PEG_{5000}-folate to DSPE-PEG_{2000} is 0:1 or 1:1) was poured into water (9 mL). This was followed by sonicating the mixture for 60 seconds at 12 W output using a microtip probe sonicator (XL2000, Misonix Incorporated, NY). The suspension was then stirred at room temperature overnight to evaporate the organic solvent. TTDNPs and FTTDNPs were assigned to NPs prepared with 0:1 and 1:1 molar ratio of DSPE-PEG_{5000}-folate to DSPE-PEG_{2000}, respectively.

Characterization: The UV-vis spectra of NP aqueous suspensions were recorded on a Shimadzu UV-1700 spectrometer. Their fluorescence spectra were measured using a fluorometer (LS-55, Perkin Elmer, USA). Average particle size and size distribution of the NPs were determined by laser light scattering (LLS) with particle

© 2012 Wiley-VCH Verlag GmbH & Co. KGaA, Weinheim

size analyzer (90 Plus, Brookhaven Instruments Co. USA) at a fixed angle of 90° at room temperature. The morphology of NPs was also studied by field emission transmission electron microscope (FE-TEM, JEM-2010F, JEOL, Japan).

Two-photon Absorption Measurements: TPA spectra were measured using two-photon induced fluorescence (TPIF) spectroscopy.[21] The samples were excited with laser pulses of 100 fs produced by the mode-locked Ti:Sapphire laser (Spectraphysics Tsunami) with a repetition rate of 82 MHz, and a femtosecond optical parametric amplifier (OPA) was used within the spectral range 800-960 nm. The emission from FTTDNP aqueous suspensions was collected at a 90° angle by a high numerical aperture lens and directed to a spectrometer's entrance slit. Rhodamine 6G in methanol was used as a reference. TPA cross section was calculated from equation:[22] $\frac{\delta_2}{\delta_1} = \frac{F_2\eta_1 c_1 n_1}{F_1\eta_2 c_2 n_2}$ where δ_1 and δ_2 are the TPA cross sections, F_1 and F_2 are the TPIF intensities, η_1 and η_2 are the fluorescence quantum yields, c_1 and c_2 are the concentrations, n_1 and n_2 are the refractive indexes of solvents (1 corresponds to Rhodamine 6G, 2 is FTTDNP). The concentration of FTTDNP suspension is calculated based on NP.

Cell Culture: MCF-7 breast cancer cells were cultured in folate-free Dulbecco's Modified Eagle Medium (DMEM) containing 10% fetal bovine serum and 1% penicillin streptomycin at 37 °C in a humidified environment containing 5% CO_2. Before experiment, the cells were pre-cultured until confluence was reached.

Cytotoxicity of FTTDNPs: The metabolic activity of MCF-7 breast cancer cells was evaluated using methylthiazolyldiphenyl-tetrazolium (MTT) assays. MCF-7 cells were seeded in 96-well plates (Costar, IL, USA) at an intensity of 4×10^4 cells·mL^{-1}. To eliminate the UV-vis absorption interference of the FTTDNPs at 570 nm, the cells incubated with the FTTDNPs without post-treatment with MTT were used as the control. After 24 h incubation, the medium was replaced by the FTTDNP suspension at different TPE-TPA-DCM concentration, and the cells were then incubated for 12, 24 and 48 h, respectively. After the designated time intervals, the wells were washed three times with 1 × PBS buffer and 100 μL of freshly prepared MTT (0.5 mg·mL^{-1}) solution in culture medium was added into each well. The MTT medium solution was carefully removed after 3 h incubation in an incubator. DMSO (100 μL) was then added into each well and the plate was gently shaken for 10 minutes at room temperature to dissolve all the precipitates formed. The absorbance of MTT at 570 nm was monitored by the microplate reader (Genios Tecan) after subtracting the absorbance of the corresponding control cells incubated with FTTDNP at the same concentration but without the addition of MTT to eliminate the absorbance interference from TPE-TPA-DCM. Cell viability was expressed by the ratio of absolute absorbance of the cells incubated with FTTDNP suspension to that of the cells incubated with culture medium only.

One-photon and Two-photon Excited In Vitro Cellular Imaging: MCF-7 breast cancer cells were cultured in the confocal imaging chambers (LAB-TEK, Chambered Coverglass System) at 37 °C. After 80% confluence, the medium was removed and the adherent cells were washed three times with 1 × PBS buffer. The TTDNPs and FTTDNPs in FBS-free DMEM medium with 0.1 nM NPs were then added to the chambers, respectively. After incubation for 2 h, the cells were washed three times with 1 × PBS buffer and then fixed with 75% ethanol for 20 minutes, which were further washed three times with 1 × PBS buffer and stained by DAPI for 10 minutes. The cell monolayer was then washed three times with 1 × PBS buffer and imaged by confocal laser scanning microscope (CLSM, Zeiss LSM 410, Jena, Germany) with imaging software (Olympus Fluoview FV1000) under the same experimental condition. The fluorescence signal from NPs was collected with a 650 nm long pass barrier filter upon excitation at 488 nm. Two-photon fluorescence images of MCF-7 breast cancer cells after incubation with TTDNPs and FTTDNPs were studied by Leica TCS SP 5X and multiphoton microscope equipped with two-photon Chameleon Ultra II, respectively. The detection of TPA fluorescence is achieved by excitation at 800 nm (~13 mW) with a 600-780 nm bandpass filter.

Uptake Mechanism Study of FTTDNPs: Cells were plated in culture flask and grown to the desired confluence. The cells incubated with 0.1 nM FTTDNPs for 2 h at 37 °C were used as the control. To study low temperature uptake efficiency, the cells were incubated with 0.1 nM FTTDNPs for 2 h at 4 °C. To study the competitive effect of free folic acid on the endocytosis of FTTDNPs, the cells were firstly incubated with 50 μg•mL^{-1} of free folic acid in DEME medium, which were followed by incubation with FBS-free DMEM medium containing 0.1 nM FTTDNPs for 2 h at 37 °C. To study the detailed endocytic mechanism, the cells were pre-treated with various inhibitors, including LY294002 (20 μg·mL^{-1}), chlorpromazine (1 μg·mL^{-1}), genistein (10 μg·mL^{-1}) and nocodazole (5 μg·mL^{-1}) for 30 minutes. The pre-treated cells were then washed three times with 1 × PBS and further incubated with 0.1 nM FTTDNP suspensions for 2 h at 37 °C. The fluorescence intensities of cells incubated under different conditions were analyzed by flow cytometry measurements using Cyan-LX (DakoCytomation) and the mean fluorescence was determined by counting 10,000 events (λ_{ex} = 488 nm, 680/20 nm bandpass filter). Statistical analysis of the mean fluorescence intensity for each group of cells was compared with the control group to obtain the corresponding relative uptake efficiency.

One-photon Excited In Vivo Fluorescence Imaging: The animal experiments for one-photon excited studies were performed in compliance with guidelines set by the Animal Care Committee at Drum-Tower Hospital. Male ICR mice implanted with murine hepatic carcinoma cell line H22 were used to investigate the *in vivo* imaging of the FTTDNPs and TTDNPs. H22 tumor cells (5–6 × 10^6 cells per mouse) were inoculated subcutaneously to the ICR mice at the right waist. H22 tumor-bearing mice were intravenously injected with 100 μL of 1 nM FTTDNPs and TTDNPs, respectively, when the tumor volume reached a mean size of about 300 mm^3. For *in vivo* fluorescence imaging, the mice were anesthetized and placed on an animal plate heated to 37 °C. The time-dependent biodistribution in mice was imaged using the Maestro *in vivo* fluorescence imaging system (CRi Inc.). Light with a central wavelength at 523 nm was selected as the excitation source. *In vivo* spectral imaging from 560 to 800 nm at 10 nm steps was conducted with an exposure time of 150 ms for each image frame. Autofluorescence was removed by using spectral unmixing software. Scans were carried out at 1 h, 6 h and 12 h post-injection.

Two-photon Excited Ex Vivo Tumor Imaging: The animal experiments for two-photon excited *ex vivo* study were performed in complicance with guidlines set by the Institutional Animal Care and Use Committee (IACUC), Singapore General Hospital. C6 glioma cell suspension containing 1 × 10^6 cells (0.1 mL) was injected subcutaneously to the left flank of BALB/c nude mice. When the tumor volume reached a mean size of ~200 mm^3, the

© 2012 Wiley-VCH Verlag GmbH & Co. KGaA, Weinheim

NANO MICRO small

mice were intratumorally injected with 100 µL of 1 nM FTTDNPs. At 24 h post-injection, the tumor tissues were excised, fixed in 4% paraformaldehyde and then imaged by Leica TCS SP 5X and multiphoton microscope equipped with two-photon Chameleon Ultra II. Two-photon excited fluorescence images of consecutive layers with 3 µm per layer were recorded to generate 3D reconstruction to investigate the penetration depth of fluorescence from FTTDNPs under excitation upon 800 nm (~39 mW) with a 600-780 nm band-pass filter.

Supporting Information

Supporting Information is available from the Wiley Online Library or from the author.

Acknowledgements

Mr. J. Geng and Dr. K. Li contributed equally to this work. We are grateful to the financial support from the Singapore National Research Foundation (R-279-000-323-281), the Institute of Materials Research and Engineering of Singapore (IMRE/11-1C0213), the Research Grants Council of Hong Kong (603509 and HKUST2/CRF/10), the Temasek Defence Systems Institute of Singapore (R279-000-305-592/422/232), the Innovation and Technology Commission of Hong Kong (ITP/008/09NP), and the University Grants Committee of Hong Kong (AoE/P-03/08). Mr. J. Geng thanks the National University of Singapore via a research scholarship.

[1] a) R. Weissleder, *Nat. Rev. Cancer* **2002**, *2*, 11; b) V. R. Kondepati, H. M. Heise, J. Backhaus, *Anal. Bioanal. Chem.* **2008**, *390*, 125; c) P. N. Prasad, *Introduction to Biophotonics* John Wiley & Sons, Hoboken, NJ.

[2] a) D. R. Larson, W. R. Zipfel, R. M. Williams, S. W. Clark, M. P. Bruchez, F. W. Wise, W. W. Webb, *Science* **2003**, *300*, 1434; b) F. Helmchen, W. Denk, *Nat. Methods* **2005**, *2*, 932; c) G. He, L. S. Tan, Q. Zheng, P. N. Prasad, *Chem. Rev.* **2008**, *108*, 1245.

[3] M. Albota, D. Beljonne, J. L. Bredas, J. E. Ehrlich, J. Y. Fu, A. A. Heikal, S. E. Hess, T. Kogej, M. D. Levin, S. R. Marder, D. McCord-Maughon, J. W. Perry, H. Rockel, M. Rumi, C. Subrananiam, W. W. Wed, X. L. Wu, C. Xu, *Science* **1998**, *281*, 1653.

[4] a) H. Y. Woo, B. Liu, B. Kohler, D. Korystov, A. Mikhailovsky, G. C. Bazan, *J. Am. Chem. Soc.* **2005**, *127*, 14721; b) H. Y. Woo, J. W. Hong, B. Liu, A. Mikhailovsky, D. Korystov, G. C. Bazan, *J. Am. Chem. Soc.* **2005**, *127*, 820.

[5] a) Q. Zheng, T. Y. Ohulchanskyy, Y. Sahoo, P. N. Prasad, *J. Phys. Chem. C* **2007**, *111*, 16846; b) W. J. Kim, A. C. Bonoiu, T. Hayakawa, C. Xia, M. Kakimoto, H. E. Pudavar, K. S. Lee, P. N. Prasad, *Int. J. Pharm.* **2009**, *376*, 141; c) Y. Q. Tian, C. Y. Chen, Y. J. Cheng, A. C. Yong, N. M. Tucker, A. K. Y. Jen, *Adv. Funct. Mater.* **2007**, *17*, 1691; d) M. Velusamy, J. Y. Shen, J. T. Lin, Y. C. Lin, C. C. Hsieh, C. H. Lai, C. W. Lai, M. L. Ho, Y. C. Chen, P. T. Chou, J. K. Hsiao, *Adv. Funct. Mater.* **2009**, *19*, 2388.

[6] a) J. D. Luo, Z. L. Xie, J. W. Y. Lam, L. Cheng, H. Y. Chen, C. F. Qiu, H. S. Kwok, X. W. Zhan, Y. Q. Liu, D. B. Zhu, B. Z. Tang, *Chem. Commun.* **2001**, 1740; b) Z. Zhao, Z. Wang, P. Lu, C. Y. K. Chan, D. Liu, J. W. Y. Lam, H. H. Y. Sung, I. D. Williams, Y. Ma, B. Z. Tang, *Angew. Chem. Int. Ed.* **2009**, *48*, 7608; c) Y. N. Hong, J. W. Y. Lam, B. Z. Tang, *Chem. Commun.* **2009**, 4332; d) Y. Liu, Y. Tang, N. N. Barashkov, I. S. Irgibaeva, J. W. Y. Lam, R. Hu, D. Birimzhanova, Y. Yu, B. Z. Tang, *J. Am. Chem. Soc.* **2010**, *132*, 13951; e) Y. Jiang, Y. C. Wang, J. L. Hua, J. Tang, B. Li, S. X. Qian, H. Tian, *Chem. Commun.* **2010**, *46*, 4689; f) Y. Liu, C. Deng, L. Tang, A. Qin, R. Hu, J. Z. Sun, B. Z. Tang, *J. Am. Chem. Soc.* **2011**, *133*, 660; g) Y. Hong, J. W. Y. Lam, B. Z. Tang, *Chem. Soc. Rev.* **2011**, *40*, 5361.

[7] a) S. Kim, H. E. Pudavar, A. Bonoiu, P. N. Prasad, *Adv. Mater.* **2007**, *19*, 3791; b) X. H. Wang, A. R. Morales, T. Urakami, L. F. Zhang, M. V. Bonder, M. Komatsu, K. D. Befield, *Bioconjugated Chem.* **2011**, *22*, 1438; c) R. B. Zhang, E. Rothenberg, G. Fruhwirth, P. D. Simonson, F. F. Ye, I. Golding, T. Ng, W. Lopes, P. R. Selvin, *Nano Lett.* **2011**, *11*, 4074.

[8] K. Li, Y. Jiang, D. Ding, X. Zhang, Y. Liu, J. Hua, S. S. Feng, B. Liu, *Chem. Commun.* **2011**, *47*, 7323.

[9] a) C. K. Lim, S. Kim, I. C. Kwon, C. H. Ahn, S. Y. Park, *Chem. Mater.* **2009**, *21*, 5819; b) K. Y. Pu, K. Li, B. Liu, *Adv. Funct. Mater.* **2010**, *20*, 2770; c) D. Ding, K. Li, Z. S. Zhu, K. Y. Pu, Y. Hu, X. Q. Jiang, B. Liu, *Nanoscale* **2011**, *3*, 1997.

[10] S. B. Noh, R. H. Kim, W. J. Kim, S. Kim, K. S. Lee, N. S. Cho, H. K. Shim, H. E. Pudavar, P. N. Prasad, *J. Mater. Chem.* **2010**, *20*, 7422.

[11] W. Qin, D. Ding, J. Liu, W. Z. Yuan, Y. Hu, B. Liu, B. Z. Tang, *Adv. Funct. Mater.* **2012**, *22*, 771–779.

[12] a) D. Wang, J. Qian, S. He, J. S. Park, K. S. Lee, S. Han, Y. Mu, *Biomaterials* **2011**, *32*, 5880; b) P. K. Kandel, L. P. Fernando, P. C. Ackroyd, K. A. Christensen, *Nanoscale* **2011**, *3*, 1037.

[13] J. M. Drake, M. L. Lesiecki, D. M. Camaioni, *Chem. Phys. Lett.* **1985**, *113*, 530.

[14] N. S. Makarov, M. Drobizhev, A. Rebane, *Opt. Express* **2008**, *16*, 4029.

[15] a) D. R. Larson, W. R. Zipfel, R. M. Williams, S. W. Clark, M. P. Bruchez, F. W. Wise, W. W. Webb, *Science* **2003**, *300*, 1434; b) E. Ishow, A. Brosseau, G. Clavier, K. Nakatani, P. Tauc, C. Fiorini-Debuisschert, S. Neveu, O. Sandre, A. Léaustic, *Chem. Mater.* **2008**, *20*, 6597; c) V. Parthasarathy, S. Fery-Forgues, E. Campioli, G. Recher, F. Terenziani, M. Blanchard-Desce, *Small* **2011**, *7*, 3219.

[16] a) S. Gottschalk, R. J. Cristiano, L. C. Smith, S. L. C. Woo, *Gene Therapy* **1994**, *1*, 185; b) K. Li, J. Pan, S. S. Feng, A. W. Wu, K. Y. Pu, Y. T. Liu, B. Liu, *Adv. Funct. Mater.* **2009**, *19*, 3535; c) J. L. Geng, K. Li, K.-Y. Pu, D. Ding, B. Liu, *Small* **2012**, DOI: 10.1002/smll.201102353.

[17] a) S. K. Lai, K. Hida, S. T. Man, C. Chen, C. Machamer, T. A. Schroer, J. Hanes, *Biomaterials* **2007**, *28*, 2876; b) T. C. Lu, J. Sun, X. X. Chen, P. B. Zhang, X. B. Jing, *Macromol. Biosci.* **2009**, *9*, 1059; c) K. Li, K.-Y. Pu, L. Cai, B. Liu, *Chem. Mater.* **2011**, *23*, 2113; d) Z. B. Liu, Z. R. Zhong, G. Peng, S. R. Wang, X. Du, D. M. Yan, Z. R. Zhang, Q. He, J. Liu, *Drug Deliv.* **2009**, *16*, 341.

[18] a) I. A. Khalil, K. Kogure, H. Akita, H. Harashima, *Pharmacol. Rev.* **2006**, *58*, 32; b) G. J. Doherty, H. T. McMahon, *Ann. Rev. Biochem.* **2009**, *78*, 857; c) B. D. Chithrani, A. A. Ghazani, W. C. W. Chan, *Nano Lett.* **2006**, *6*, 662.

[19] a) Y. Mo, L. Y. Lim, *J. Pharm. Sci.* **2004**, *93*, 20; b) R. G. W. Anderson, B. A. Kamen, K. G. Rothberg, S. W. Lacey, *Science* **1992**, *255*, 410; c) C. Mineo, R Anderson, *Histochem. Cell Biol.* **2001**, *116*, 109.

[20] N. Araki, M. T. Johnson, J. A. Swanson, *J. Cell Biol.* **1996**, *135*, 1249.

[21] C. Xu, W. W. Webb, *J. Opt. Soc. Am. B* **1996**, *13*, 481.

[22] D. A. Oulianov, I. V. Tomov, A. S. Dvornikov, P. M. Rentzepis, *Opt. Commun.* **2001**, *191*, 235.

Received: April 16, 2012
Revised: June 22, 2012
Published online: August 15, 2012

 © 2012 Wiley-VCH Verlag GmbH & Co. KGaA, Weinheim